Accelerated Publications

Coherent Dynamics during the Primary Electron-Transfer Reaction in Membrane-Bound Reaction Centers of *Rhodobacter sphaeroides*†

Marten H. Vos,‡ Michael R. Jones,§ C. Neil Hunter,§ Jacques Breton,| Jean-Christophe Lambry,‡ and Jean-Louis Martin*,‡

Laboratoire d'Optique Appliquée, Ecole Polytechnique-ENSTA, INSERM U275, CNRS URA 1406, 91120 Palaiseau, France, Krebs Institute for Biomolecular Research and Robert Hill Institute for Photosynthesis, Department of Molecular Biology and Biotechnology, University of Sheffield, Western Bank, Sheffield S10 2UH, United Kingdom, and SBE/DBCM, CEN de Saclay, 91191 Gif-sur-Yvette Cedex, France

Received March 11, 1994; Revised Manuscript Received March 31, 1994®

ABSTRACT: The temporal evolution of the near-infrared stimulated emission band of the special pair excited state (P*) in the reaction center of *Rhodobacter sphaeroides* has been studied in intracytoplasmic membranes of the antenna-deficient RCO1 mutant at 10 K with a resolution of 30 fs. On the 100-fs time scale the emission band gradually shifts to longer wavelengths. After 150 fs the band shifts back to shorter wavelengths and continues to develop on the picosecond time scale in a damped oscillatory manner (most prominent fundamental frequencies around 15 cm^{-1} and at 92, 122, and 153 cm^{-1}). These phenomena are shown to be due to low-frequency vibrational motions in the P* excited state that conserve their phase on the time scale of electron transfer. These results imply that the vibrational manifold of P* is not thermalized during the electron-transfer reaction in functional reaction centers. The initial Stokes shift dynamics are largely determined by the modes in the 90–160-cm^{-1} frequency range, which probably involve motions of several chromophores, including the bacteriopheophytin electron acceptor H_L.

The primary charge separation in bacterial photosynthesis occurs from the lowest lying excited state P* of the hexachromophoric reaction center protein. P* decays very rapidly toward a state of interchromophore charge separation. This process takes place mainly in a few picoseconds at room tempearture and somewhat faster (~1 ps) at cryogenic temperatures [for a review, see Martin and Vos (1992)]. Fluorescence emission from P* is red-shifted (Stokes-shifted) from the position of the corresponding ground-state P absorption band. Stokes-shifted (400–500 cm^{-1}) stimulated (Martin et al., 1986; Woodbury et al., 1985) and spontaneous (Du et al., 1992; Hamm et al., 1993) emission from P* has been observed on the picosecond and subpicosecond time scale. This large Stokes shift implies that prior to charge separation, i.e., on the femtosecond time scale, the nuclear configuration of the chromophore–protein complex is significantly altered [see, for example, Middendorf et al. (1991)].

The onset of the Stokes shift is directly related to the properties of the modes that couple most strongly to the P → P* optical transition and that may also assist the very efficient electron-transfer process. However, until now the kinetics of the Stokes shift have not been directly resolved in femtosecond studies. Important insight in the vibrational structure underlying the P absorption band has been obtained with steady-state techniques, i.e., photochemical hole burning and resonance Raman. From these studies it was concluded that low-frequency vibrational modes (<150 cm^{-1}) couple most strongly to the P → P* optical transition. The interpretation of hole-burning data from different studies (Johnson et al., 1990; Lyle et al., 1993; Middendorf et al., 1991) requires a minimum of two low-frequency modes (near 30 and 130 cm^{-1}). Shreve et al. (1991) and Palaniappan et al. (1992) observed at least five strong Raman bands up to 200 cm^{-1} upon direct excitation of P, although the detailed spectra of these two studies are remarkably different. The conclusion that the low-frequency modes couple most strongly to the P → P* transition corresponds well with the frequency range of the oscillatory features (15–80 cm^{-1}) that we previously observed in the stimulated emission of wild-type (WT) and mutant reaction centers and that we have shown to be due to coherent vibrational motion (Vos et al., 1991, 1993). The experimentally observed dephasing times, which set a lower limit to the coherence times, are in the order of 1 ps. These are in general agreement with the time dependence of correlations between atom positions in proteins inferred from molecular dynamics calculations (Karplus & McCammon, 1983; Smith, 1991). Also, correlation functions derived from molecular dynamic simulations specifically of the reaction center protein show low-frequency oscillatory behavior (Warshel et al., 1989; Warshel & Parson, 1991; Schulten & Tesch, 1991; Gehlen et al., 1994).

Nuclear dynamics play an essential role in the electron-transfer reactions as they allow the system to reach the nuclear configuration where the energy gap between the donor state and the charge-separated state vanishes and where curve crossing of the donor- and product-state potential energy surfaces may take place [cf. Gehlen et al. (1994)]. For vibrationally relaxed states the nuclear configuration space is thermally populated, and electron transfer is brought about

† M.H.V. was supported by CEN, CNRS, and Fondation pour la Recherche Médicale during the course of this work. M.R.J. and C.N.H. acknowledge support from the Wellcome Trust and the European Community. M.R.J. is an AFRC Senior Research Fellow.

‡ INSERM U275, CNRS URA 1406.
§ University of Sheffield.
| CEN de Saclay.

® Abstract published in *Advance ACS Abstracts,* May 1, 1994.

0006-2960/94/0433-6750$04.50/0

by stochastic dynamics and can be phenomenologically described with a simple rate constant. This is the regime of nuclear motion assumed in conventional electron-transfer theory (Marcus & Sutin, 1985). This theory has been applied to many biological electron-transfer reactions (Moser et al., 1992) as a general rule.

A different regime may apply for ultafast electron-transfer reactions if the phase of vibrational motion assisting electron transfer persists on the time scale of the reaction. In this case the curve-crossing region is reached in a concerted way, and the electron transfer macroscopically proceeds in an oscillatory manner in time. This regime has been evoked by Jortner (1980), and recent theoretical studies have indicated that a coherent regime of electron transfer may be at the origin of the extreme efficiency and speed of the primary electron-transfer step in photosynthesis (Jean et al., 1992; Skourtis et al., 1992). Therefore, it is important to identify the nature of the nuclear motions immediately after the population of P*.

In a femtosecond-stimulated emission study, we have recently shown that for reaction centers of the D_{LL} mutant of *Rhodobacter capsulatus*, which are incapable of electron transport, the activated low-frequency motions are in a coherent regime on the time scale of electron transfer in functional reaction centers (Vos et al., 1993). In the present study, we concentrate on the time evolution of the stimulated emission band of WT reaction centers from *Rhodobacter sphaeroides*. Some changes in experimental approach have been introduced compared to our previous work on WT reaction centers (Vos et al., 1991, 1992). To ensure an optimally homogeneous and natural environment for the reaction center protein, we used membranes from the antenna-deficient RCO1 mutant of *R. sphaeroides* (Jones et al., 1992), where the oscillatory features persist longer than in detergent-isolated reaction centers (to be published). Furthermore, we significantly extended the bandwidth of the accessible vibrational frequency range (to $\sim$300 cm^{-1}) by using spectrally broader and shorter (30 fs) pump pulses. Finally, we scanned the entire stimulated emission band using an external calibration of the absolute zero time delay at each wavelength. These improvements have allowed us to observe new and important features, including a time-resolved coherent Stokes shift at both cryogenic and room temperature, and oscillatory features near 120 cm^{-1}. This paper describes the results at low temperature.

MATERIALS AND METHODS

Intracytoplasmic membranes from the *R. sphaeroides* RCO1 mutant, in which the genes coding for both the LHI and LHII antenna proteins are deleted, were prepared as described (Jones et al., 1992) and suspended in 20 mM Tris buffer, pH 8.0. The samples were mixed with 50% glycerol (v/v). The concentration of the sample was adjusted to an optical density of $\sim$0.35 at 860 nm at room temperature (optical path length 1 mm). Then 50 mM dithiothreitol was added to prereduce the electron acceptor Q_A. The measurements were done at 10 and 100 K in a convection cryostat.

For purposes of calibration of the zero time delay (see below), isolated reaction centers of *Rhodopseudomonas viridis* were used at room temperature. These were prepared as described (Breton, 1985) and suspended in 10 mM Tris, pH 8.0, and had an optical density of $\sim$0.5 at 950 nm.

The femtosecond spectrometer was essentially as described previously (Vos et al., 1992). The pump pulses were centered at 870 nm. Unless mentioned otherwise, the shaping of the pulses and their resulting characteristics were as follows. A pulse width of $\sim$30 fs full width at half-maximum (fwhm) was obtained by amplifying a white light continuum using the dye LDS 867 in a mixture of ethanol and propylene carbonate (2%) and compressing using a pair of SF10 prisms. Pump spectral components below $\sim$850 nm and above $\sim$905 nm were filtered with a Corion LL850 cutoff filter and by spatial filtering in the Fourier transform plane of the compressor, yielding a spectral fwhm of $\sim$30 nm.

The probe beam was also compressed to less than 30 fs using SF10 prisms. The instrument response function was essentially determined by the length of the pump pulse at each wavelength in the spectral region under study. The compression of the probe beam was fine-tuned by careful determination of the zero time delay in the instantaneous bleaching kinetics at different wavelengths of the P band of reaction centers of *R. viridis*, which covers, at room temperature, the entire spectral range of this study. This procedure yielded the expected approximately parabolic dispersion curves (Fork et al., 1984), corresponding to a parabolically chirped probe pulse, in which the optimally compressed wavelength component arrives at the sample first. In this way, the temporal dispersion was compressed to less than 10 fs over a 40-nm spectral region around the central compression wavelength and to less than 40 fs over a 100-nm spectral region. For the spectra the probe pulses were compressed at $\sim$920 nm. For the kinetics, the probe pulses were optimally compressed at a wavelength less than 20 nm from the detection wavelength. This allowed us to determine the relative position of the zero time delay for the kinetics at different wavelengths within a 40-nm region with an accuracy of $\sim$10 fs (this time corresponds to a 1.5 μm movement of the delay line and is limited by the long-time mechanical stability of our setup). For the *R. sphaeroides* samples studied at cryogenic temperatures, an absolute determination of the zero time delay with an accuracy better than 20 fs was obtained by monitoring kinetics in the region of bleaching of the P band with the same compression setting and comparison with the compression curve obtained as described above.

The stimulated emission of the *R. sphaeroides* RCO1 membranes itself could not be used to tune the compression of the probe pulse, because it does not appear instantaneously after excitation (see Results section). Conversely, the failure to obtain parabolic curves of apparent zero time delay versus wavelength in the stimulated emission region of the *R. sphaeroides* samples indicates that its rise is wavelength-dependent.

Kinetic scans were taken either on a 1-ps full-scale time base (one point per 13 fs) or on a dual 4- and 46-ps full-scale, time base (one point per 33 fs and 2.3 ps, respectively). The latter data were analyzed by fitting to multiexponential decay functions over a kinetic stretch starting after the first maximum of the stimulated emission and including data of the two time bases. Fourier transform (FT) vibrational spectra (resolution 8 cm^{-1}) of the residuals (oscillatory parts) of the 4-ps full-scale time base part of this kinetic stretch, zero-filled to 128 points, were obtained using the fast Fourier transform algorithm.

RESULTS

Figure 1 shows the 10 K transient absorption spectra in the P band absorption and stimulated emission region at different delay times. The high time resolution and the minimized chirp in combination with the high signal to noise ratio of the transient spectra allow us to observe several hitherto unresolved

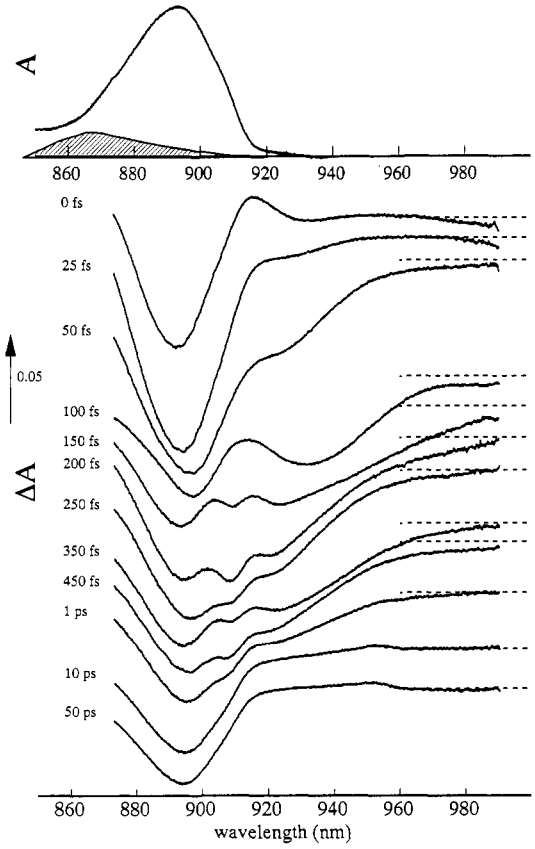

FIGURE 1: Ground-state absorption spectrum (upper panel) and transient absorption spectra at various delay times at 10 K. The jitter in the timing of the spectra is <10 fs and the systematic error in the delay times <20 fs. The hatched curve in the upper panel represents the spectrum of the pump pulse.

features. Most importantly, we have time resolved the Stokes shift of the stimulated emission. At very early times (up to ~50 fs) the transient signal is dominated by a bleaching feature in the P band region, centered at approximately 895 nm at 50 fs. This bleaching feature relaxes in part within 100 fs, and a signal to the red of the P band rises on this time scale. This band, generally attributed to $P^* \rightarrow P$ stimulated emission (Martin et al., 1986; Woodbury et al., 1985), gradually shifts to the red and achieves a maximal red shift after about 150 fs. Subsequently, it shifts back to the blue and keeps shifting and changing its form in an oscillatory manner up to more than 1 ps. On the picosecond time scale the overall intensity of the stimulated emission band decreases due to decay of P* to the charge-separated state $P^+H_L^-$.

These data clearly show that the maximal amplitude of the Stokes shift takes place on a time scale of about 100 fs in a coherent way. A low-frequency mode appears to be mainly responsible for the Stokes shift, and this mode is not dephased on the time scale of the progression of the emission to the most red-shifted wavelength. This point is further illustrated by the subpicosecond kinetics shown in Figure 2. The first maximum of the signal appears later for longer wavelengths, and generally second maxima appear ~280 fs after the first, corresponding to a frequency of ~120 cm^{-1}. The phases of the oscillations on the red and blue sides of the stimulated emission band are opposite, and the oscillations vanish near the center of the band (~918 nm). Such features have been observed for lower frequency modes in the D_{LL} mutant of *R. capsulatus* (Vos et al., 1993), and they show that the oscillatory features are due to coherent excited-state vibrations.

After 150 fs the stimulated emission spectrum evolves into a double-banded structure with peaks at ~910 and ~925 nm. This feature has also been observed in other functional reaction center preparations (unpublished results) but not in the D_{LL} mutant of *R. capsulatus* (Vos et al., 1993). The blue-most band appears in the spectral region where the zero-phonon hole in hole-burning experiments can be observed at temperatures below 20 K (Johnson et al., 1990; Lyle et al., 1993), but this is probably fortuitous as the amplitude of the feature observed here does not depend strongly on the temperature between 5 and 20 K and is clearly visible at 100 K (not shown). We propose that the observed bimodal structure of the stimulated emission band arises as a result of the fact that P* is vibrationally unrelaxed, as will be explained in the Discussion. Accordingly, the structure disappears with the overall decay of P*.

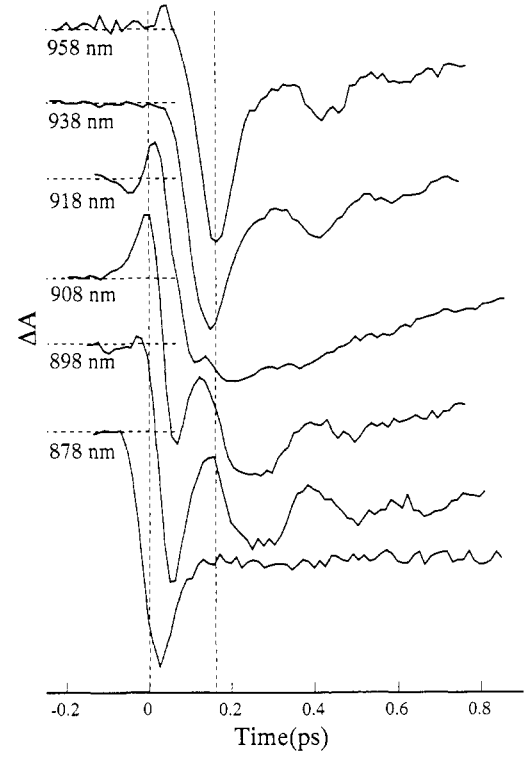

FIGURE 2: Early-time kinetics at selected wavelengths at 10 K. The amplitudes are normalized. The jitter in the timing of the kinetics is <10 fs and the systematic error in the delay times <20 fs.

On the picosecond time scale, the spectrum evolves to the ($P^+H_L^-$ – P) spectrum (almost pure at 50 ps), consisting of the bleaching of the P band and a small but significant induced absorption at the red side of this band which extends to about 955 nm. As a band in this spectral region also appears in the ($P^+Q_A^-$ – P) spectrum of isolated *R. sphaeroides* reaction centers (Parson et al., 1992; Arlt et al., 1993), it is ascribed to P^+. In accord with these observations, a similar feature is found in the Bchl *a* cation spectrum in solution (Fajer et al., 1975).

At $t = 0$ fs an apparent small induced absorption around 915 nm is observed. This feature is linear in pump energy and is not due to chirp in the probe pulse. As this feature, and a similar feature at the blue side of the P band, near 860 nm (not shown), is only seen during the pump–probe overlap time, it is probably not related to the dynamics of P* but rather to a change in the optical properties of the sample induced by the pump field. It is possibly due to the optical Stark effect, in which the electric field of the pump pulse modulates the electronic spectrum in a nonresonant way. This effect is only present when pump and probe overlap in time and is, for not extremely high fields, linear in pump intensity. Optical Stark

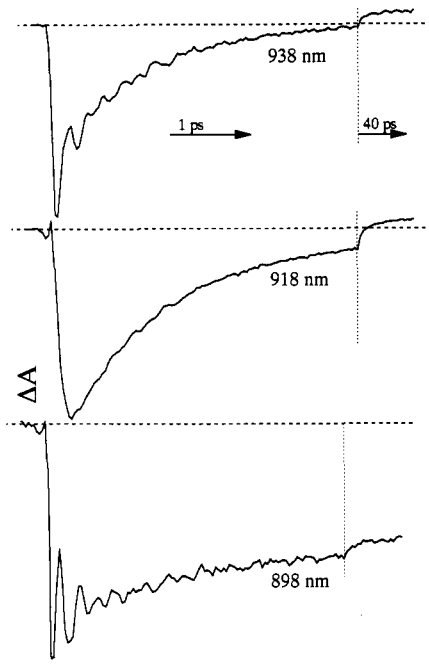

FIGURE 3: Dual time-base kinetics (4 and 46 ps) at selected wavelengths at 10 K.

effects have been observed in organic dyes (Becker et al., 1988) using pump intensities of the same order of magnitude as those used in this study (10^{10}–10^{11} W/cm^2). Furthermore, the observed features correspond qualitatively with the known steady-state Stark spectrum of P (Lösche et al., 1987; Lockhart & Boxer, 1988), and their amplitude is in the range expected for the field strength corresponding to this intensity [(2–7) × 10^6 V/cm].

Figure 3 shows, on extended time scales, the kinetics observed near the center (918 nm) and at both sides of the stimulated emission band (938 and 898 nm). Oscillatory features are observed up to at least 2 ps, the pattern being rather irregular after a few hundred femtoseconds. This indicates that a manifold of vibrational modes is activated by the pump pulse. The oscillatory features were further analyzed by subtracting exponentially decaying fit functions from the data (Figure 4). Clearly, the oscillatory patterns of the two signals at 938 and 898 nm with opposite phase resemble one another in detail (Figure 4, inset). A FT frequency analysis of the kinetics highlights a component around 15 cm^{-1} and a broad band centered at around 120 cm^{-1} with peaks superimposed at about 92, 122, 153, and 191 cm^{-1}. The 938-nm residuals further display peaks at 69 cm^{-1} (corresponding to a shoulder in the FT spectrum of the oscillations observed at 898 nm) and at 329 cm^{-1} (see also Figure 5). As discussed previously (Vos et al., 1993), the FT bands of the oscillations observed at the extremes of the stimulated emission band primarily reflect the fundamental frequencies of the activated vibrational modes. Analysis of the FT components reveals that the width of the 120-cm^{-1} band is related to the apparent relatively fast initial damping of the oscillations. FT of kinetic stretches starting at increasingly longer delay times and modeling of the kinetics with damped sinusoidal functions indicate a relatively fast damping (~200 fs) of the 122-cm^{-1} band as compared to the bands at ~92 and 153 cm^{-1} (not shown).

At 918 nm, the amplitudes of the FT bands are an order of magnitude lower than those at 898 and 938 nm, and the bands are highly congested in the region up to ~150 cm^{-1}. These results are consistent with the relative enhancement of overtones and sum and difference frequencies expected in this region (Vos et al., 1993). No FT band is observed in the 240-cm^{-1} region, where the double frequency of the fundamentals of the 120-cm^{-1} region would be expected. This may be due to a combination of the relatively strong damping of the 122-cm^{-1} band and the fact that this region is near the vibrational bandwidth limit of our experiment.

The amplitude and shape of the lowest frequency features (around 15 cm^{-1}) in the residuals depend on the details of the exponential fit subtracted from the data. However, the frequency region <35 cm^{-1} always has a significant vibrational strength, even if a three-exponential fit is used. The low-frequency feature can be better visualized by using a longer (and spectrally narrowed) pump pulse, which suppresses the high-frequency features. This is illustrated in Figure 5 with data taken at λ = 938 nm, at 100 K, where P* is somewhat longer lived (Fleming et al., 1988). These results are broadly in line with our previous data on isolated reaction centers of *R. sphaeroides* R-26 (Vos et al., 1991), where an ~15-cm^{-1} feature was observed with long (80 fs) pump pulses. This feature, together with the ~120-cm^{-1} features, can be resolved with the short pump and probe pulses used in the present study but was not resolved previously with 45-fs pulses. This difference probably stems from (a) the present improvements in time resolution, (b) the restriction of our previous study to one detection wavelength in the stimulated emission region, in the vicinity of the center of the band, and (c) the fact that the present study was conducted on membrane-bound reaction centers rather than on detergent-solubilized complexes.

Comparison of Figures 3–5 shows that the relative amplitude and the vibrational spectra of the oscillations are very similar at 10 and 100 K. We have also observed clear oscillations at room temperature. A complete account of our room temperature experiments will be published elsewhere.

DISCUSSION

The data presented here constitute the first assessment of the time dependence of the Stokes shift in bacterial reaction centers. The Stokes shift is found to appear with a half-period (time taken for the emission band to reach the lowest energy) of about 150 fs. In the kinetics, the Stokes shift appears as a delayed rise of the signal at the red side of the emission spectrum with the apparent rise time not much longer than that at the blue side of the spectrum (Figure 2). This coherent rise behavior and the related need for an independent determination of the absolute position of maximal temporal overlap between the pump and probe pulse (t = 0) has probably prevented the resolution of the time dependence of the Stokes shift in earlier studies at low temperature (Fleming et al., 1988; Breton et al., 1988; Vos et al., 1991; Lauterwasser et al., 1991; Chan et al., 1991).

The observed spectral evolution can be understood in terms of wave-packet motion on the P* potential energy surface as discussed previously for the simpler case of a nondecaying excited state (Vos et al., 1993). In Figure 6 a simplified scheme is presented, where nuclear motion is assumed to evolve along a single coordinate and where curve crossing is treated as a sink. We do not pretend to give an accurate description of coherent electron transfer with this model but rather to provide a guide in the qualitative interpretation of the early time evolution of the wave packet. Near the turning points (probed at the blue and red edges of the stimulation emission band), the wave packet passes once per vibrational period, giving rise to kinetics oscillating with the fundamental frequencies and with opposite phases for both turning points. The wave packet

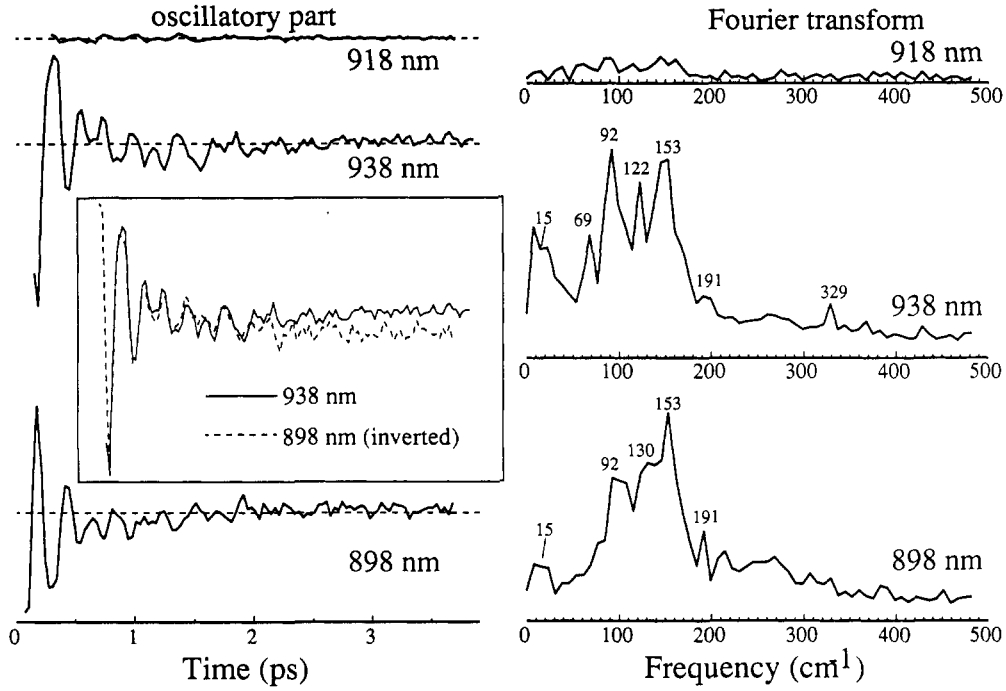

FIGURE 4: Analysis of the data in Figure 3. Oscillatory parts were obtained by fitting the data to two-exponential (898 and 938 nm) and three-exponential (918 nm) kinetics, respectively, and Fourier transformed as described in the Materials and Methods section. Inset: superposition of the oscillatory parts at 938 and 898 nm (inverted and matched).

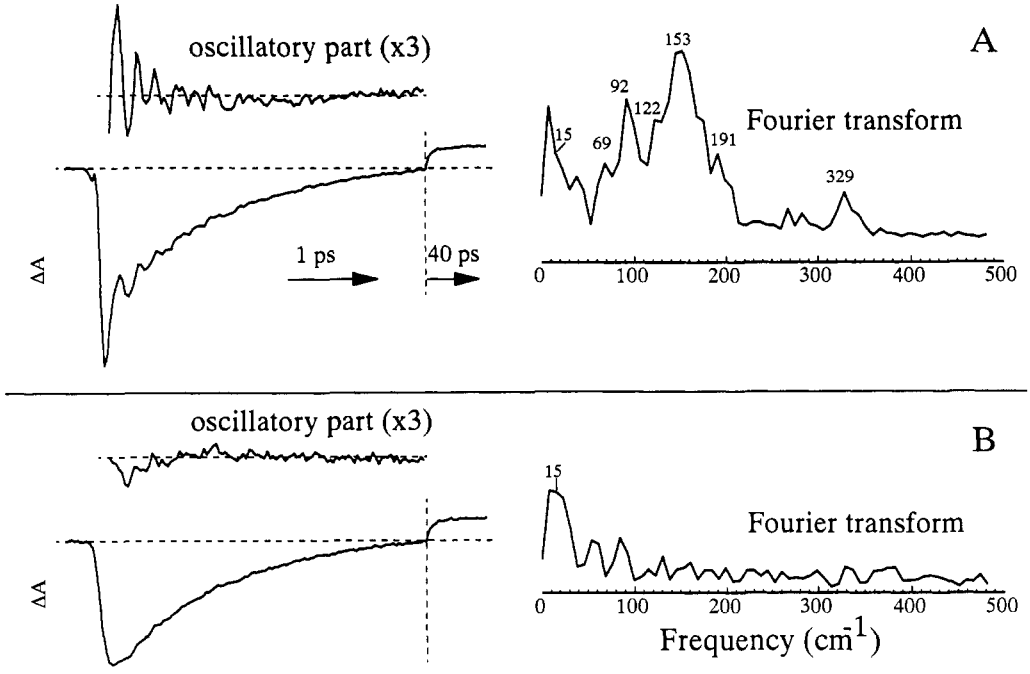

FIGURE 5: Kinetics, oscillatory parts, and FT of the kinetics at 938 nm at 100 K. Note the dual time base (4 and 46 ps). Panels: (A) 30-fs pump pulse with a spectrum as in Figure 1; (B) 100-fs pump pulse centered at 870 nm with a spectral width of 10 nm, obtained by replacing the 850-nm cutoff filter by an 870-nm interference filter.

broadens by anharmonicity and quasielastic (pure dephasing) and nonelastic (vibrational relaxation) collisions. The latter gradually reduce the amplitude of the wave-packet motion along the coordinate and may be at the origin of the observed stronger damping of the oscillations and faster decay of the overall stimulated emission observed at both extremes of the stimulated emission band (vide infra). For instance, almost no recurrence is monitored at $\lambda = 878$ nm (Figure 2), where stimulated emission is expected from the coordinate region where the wave packet is initially prepared by the pump pulse. Also, the Stokes shift associated with the first occurrence (at $t \sim 150$ fs) of the wave packet at the red-most side of the potential energy surface extends further than that associated with its first recurrence (at $t \sim 450$ fs) (Figure 1).

The FT analysis of the data at longer time scales (Figure 4) reveals a manifold of vibrational features. The strong FT features observed at both sides of the emission band that are associated with the fundamental frequencies of displaced P* (excited-state) vibrational modes can be compared with resonance Raman spectra that probe ground-state vibrational modes coupled to the optical transition. Our findings are in agreement with the general conclusion, derived from two such studies (Shreve et al., 1991; Palaniappan et al., 1992), that the P $\rightarrow$ P* transition mainly couples to low-frequency

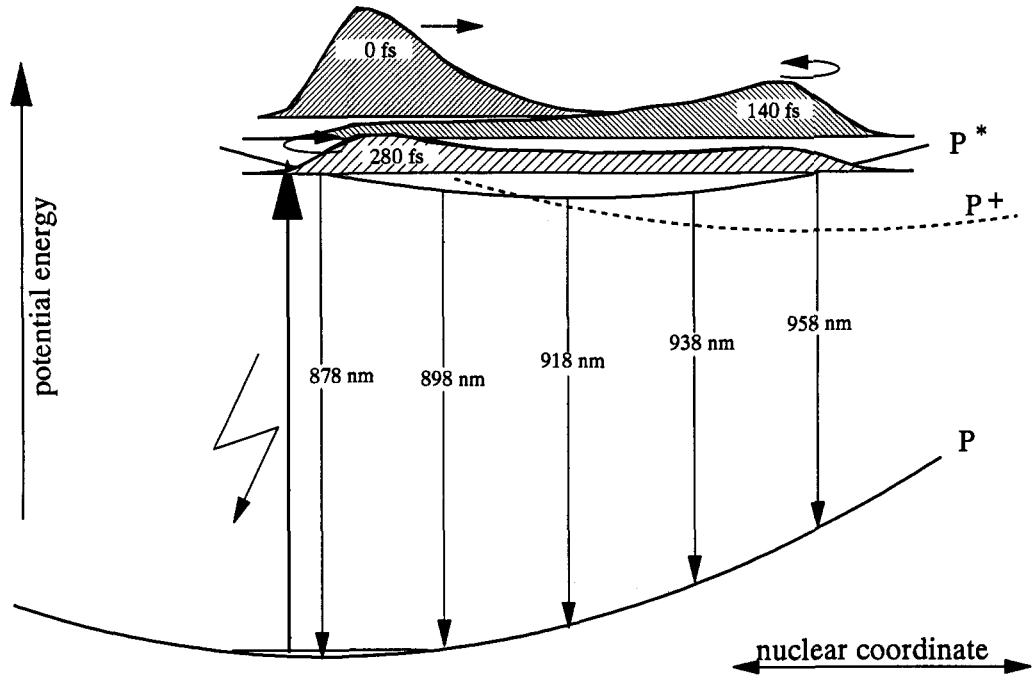

FIGURE 6: Scheme of wave packet motion along a single displaced coordinate on the 120-cm^{-1} cross section of the P* potential energy curve. For clarity, the curvature of the curves is not in scale. For harmonic and displaced ground- and excited-state surfaces the relation between stimulated emission photon energy and the probed nuclear coordinate is linear. In this simplified model, the P* state is depopulated via a sink by surface crossing to the P$^+$ charge-separated state, whose potential energy surface (dashed) is tentatively drawn to cross at the bottom of the P* well. The wave packets at t = 0, 140, and 280 fs, populated by a 30-fs pump pulse, were calculated with a simple semiclassical formalism of diffusional broadening inspired by Heller's (1981) frozen Gaussian approximation.

vibrational modes. In particular, Shreve et al. (1991) reported bands in the room temperature spectra of *R. sphaeroides* R-26 reaction centers at 71, 94, 127, 202, and 337 cm^{-1}, and these are remarkably similar to the peaks at 69, 92, 122, 191, and 329 cm^{-1} that appear in our study. The main differences constitute a Raman peak at 36 cm^{-1}, which we do not observe at low temperature, and the FT peak at 153 cm^{-1}, which does not appear in the Raman spectrum. The former was observed at the very lower limit of the accessible frequency domain and may be an overtone of, or part of, the 15-cm^{-1} feature observed in our data. An ~153-cm^{-1} band may not have been resolved in the Raman study due to spectral congestion. However, it should also be kept in mind that resonance Raman probes the *ground state* vibrational modes and, therefore, the two techniques should not *a priori* yield exactly the same vibrational information. Conversely, the apparent similarity of many of the bands suggests that the curvature of the potential energy surfaces of the ground and excited states is not very different.

The 122-cm^{-1} FT feature damps relatively rapidly (apparent dephasing time ~200 fs). It may be envisaged that this mode, which is strongly activated by the initial population of P*, is anharmonically coupled to the other modes, which dephase on a longer time scale (>500 fs). In such a view, the 122-cm^{-1} mode moves the wave packet, in a phase-conserving manner, out of the Franck–Condon region onto the multidimensional surface from which electron transfer occurs. The anharmonic coupling to a limited number of other modes prevents the wave packet returning to the initially populated Franck–Condon region. Such irreversible coherent wave-packet motion, or alternatively the vibrational relaxation of the 122-cm^{-1} mode only, may be at the origin of the fast relaxation observed in transient absorption experiments in the Q_Y spectral region of the monomeric chromophores (Vos et al., 1992). Further experiments and modeling are required to investigate these suggestions.

Modeling of photochemical hole-burning profiles of P requires, in the frequency region below 200 cm^{-1}, a minimum of two displaced modes near 120 and 30 cm^{-1} (Johnson et al., 1990; Middendorf et al., 1991; Lyle et al., 1993). These frequency ranges are in good agreement with our direct determination of the modes that are displaced in P*. The homogeneous line widths of >50 cm^{-1} required for optimal modeling of the hole-burning profiles are inconsistent with the dephasing times >200 fs that we establish here for most features but not for the 122-cm^{-1} mode which may be most activated initially, as discussed above. In addition, as discussed both by Middendorf et al. (1991) and by Lyle et al. (1993), smaller homogeneous line widths would be possible if a greater number of distinct low-frequency modes would be significantly coupled to the optical transition. Our findings of several vibrational modes with dephasing times appreciably longer than 200 fs in the vicinity of 120 cm^{-1} show that this is the case, and they may be used for more refined modeling of the hole-burning profiles. In passing, we note that the dephasing times are also somewhat longer when the reaction centers are embedded in the membrane, as in our study, than when they are detergent-isolated (to be published).

The Stokes shift dynamics at early times are predominantly due to motion along the modes associated with the 120-cm^{-1} region and not to motion along the 15-cm^{-1} mode, indicating that the 120-cm^{-1} region is largely responsible for the Franck–Condon progression of the stimulated emission band. As the Franck–Condon progression is proportional to $\sum_i S_i\omega_i$, in which S_i are the coupling strengths (Huang–Rhys factors) of modes with frequencies ω_i, this is consistent with the hole-burning modeling which predicts S's of ~2 and ~1.2 for vibrational modes in the 30- and 120-cm^{-1} regions, respectively (Johnson et al., 1990; Middendorf et al., 1991; Lyle et al., 1993). It can be excluded that higher frequency modes bear significant coupling strength, as this would lead to faster initial Stokes shift dynamics.

The dominance of the 120-cm^{-1} vibrational region in determining the vibrational structure underlying the stimulated emission band may *a posteriori* justify the use of the simplified

picture of wave-packet motion along a single nuclear coordinate as shown in Figure 6 to qualitatively illustrate the origin of observed spectral features. A striking feature in the wave-packet evolution is that, after some dephasing, it may display peaks near both turning points. This reflects the fact that, during vibrational motion, the conformation is most often close to that of either of the turning points, where the velocity vanishes. The turning points are probed at the blue and red side of the spectrum, and therefore a bimodal spectrum may be observed when the wave packet is broadening (for instance, through frequency dispersion by anharmonic coupling to an number of close-lying modes). We suggest that the bimodal character of the stimulated emission band at times >150 fs (Figure 1) is due to this effect. It is thus the direct consequence of the selective and coherent population of the higher vibrational levels. Such features are not expected in a vibrationally relaxed excited state, where the zero vibrational level, located at the bottom of the well, is most populated.

The bimodal structure is expected to smear out when inhomogeneous broadening is important. Photochemical hole-burning studies indeed indicate that the P band is mainly homogeneously broadened at low temperature (Johnson et al., 1990; Middendorf et al., 1991). The absence of a clear bimodal shape in the spectrum of the *R. capsulatus* D_{LL} mutant (Vos et al., 1993) may be due to a larger inhomogeneous broadening, which would corroborate the less steep low-energy side of the ground-state P band in this mutant. Also, the different vibrational structure underlying this band (see below) may be of influence.

The 15-cm^{-1} mode can be attributed to one (or more) global mode of the protein (Franck–Condon coupled via the chromophore system) by virtue of the low frequency (Gō et al., 1983; Karplus & McCammon, 1983). The modes in the 120-cm^{-1} region could be more localized. Vibrations of the bacteriochlorophyll (Bchl) *a* dimer constituting P may be expected in this region (Warshel, 1980), and intrachromophore modes cannot be entirely excluded as a Bchl *a* Raman mode as low as 130 cm^{-1} has been observed in solution (Lutz & Mäntele, 1991), but most probably the protein "solvent" and possibly other chromophores are also involved in those modes. In this context a comparison with the frequencies of coherent vibrations in the D_{LL} mutant from *R. capsulatus* (Vos et al., 1993) is interesting. In this mutant, which lacks the bacteriopheophytin acceptor H_L (probably located ~17 Å from P in WT *R. capsulatus* reaction centers), a peak is observed at 77 cm^{-1} rather than 120 cm^{-1}. A possible interpretation of this is that nuclear motion in the H_L region contributes to modes in the 70–120-cm^{-1} range. However, a direct comparison is complicated by the species difference between D_{LL} and RCO1 and the fact that the D_{LL} mutation involved a helix swap which is the equivalent of 11 site-directed changes, including several residues in the vicinity of P.

Our present results show that the manifold of vibrational modes activated by the formation of P* is not thermalized on the time scale of electron transfer in WT reaction centers. Thus the excited state does not relax to the zero phonon level prior to electron transfer, as has been suggested from the correlation between the apparent lifetime of P* and the width of the zero-phonon hole [Johnson et al., 1989; Lyle et al., 1993, see also Middendorf et al. (1991)]. Although it is possible that the $P^* \rightarrow P^+H_L^-$ charge separation is assisted by motions orthogonal to those activated by the $P \rightarrow P^*$ transition, it is tempting to speculate that the activation of a few specific low-frequency modes is directly related to the charge separation reaction. A detailed study of spectral regions probing the product state(s) is needed to investigate this point.

In conclusion, we have shown that the Stokes shift in functional reaction centers appears in a coherent manner, due to nuclear motion along the coordinate of modes in the 120-cm^{-1} region. We have established that essentially all modes that are significantly coupled to the $P \rightarrow P^*$ transition are low-frequency modes which keep phase correlations on the time scale of depopulation of the excited state by electron transfer. Therefore, in P*, the nuclear motions with the largest amplitudes are not thermally relaxed during the very efficient physiological electron-transfer reaction. Theoretical models describing the primary electron transfer should be adapted to predict the proper description of the time evolution of the system in the P* precursor state, even in the hypothesis that the reaction coordinates are orthogonal to those motions.

REFERENCES

Arlt, T., Schmidt, S., Kaiser, W., Lauterwasser, C., Meyer, M., Scheer, H., & Zinth, W. (1993) *Proc. Natl. Acad. Sci. U.S.A. 90*, 11757–11761.

Becker, P. C., Fork, R. L., Brito Cruz, C. H., Gordon, J. P., & Shank, C. V. (1988) *Phys. Rev. Lett. 60*, 2462–2464.

Breton, J. (1985) *Biochim. Biophys. Acta 810*, 235–245.

Breton, J., Martin, J.-L., Fleming, G. R., & Lambry, J.-C. (1988) *Biochemistry 27*, 8276–8284.

Chan, C.-K., DiMagno, T. J., Chen, L. X.-Q., Norris, J. R., & Fleming, G. R. (1991) *Proc. Natl. Acad. Sci. U.S.A. 88*, 11202–11206.

Du, M., Rosenthal, S. J., Xie, X., DiMagno, T. J., Schmidt, M., Hanson, D. K., Schiffer, M., Norris, J. R., & Fleming, G. R. (1992) *Proc. Natl. Acad. Sci. U.S.A. 89*, 8517–8521.

Fajer, J., Brune, D. C., Davis, M. S., Forman, A., & Spaulding, L. D. (1975) *Proc. Natl. Acad. Sci. U.S.A. 72*, 4956–4960.

Fleming, G. R., Martin, J.-L., & Breton, J. (1988) *Nature 333*, 190–192.

Fork, R. L., Martinez, O. E., & Gordon, J. P. (1984) *Opt. Lett. 9*, 150–152.

Gehlen, J. N., Marchi, M., & Chandler, D. (1994) *Science 263*, 499–502.

Gō, N., Noguti, T., & Nishikawa, T. (1983) *Proc. Natl. Acad. Sci. U.S.A. 80*, 3696–3700.

Hamm, P., Gray, K. A., Oesterhelt, D., Feick, R., Scheer, H., & Zinth, W. (1993) *Biochim. Biophys. Acta 1142*, 99–105.

Heller, E. J. (1981) *J. Chem. Phys. 75*, 2923–2931.

Jean, J. M., Friesner, R. A., & Fleming, G. R. (1992) *J. Chem. Phys. 96*, 5827–5842.

Johnson, S. G., Tang, D., Jankowiak, R., Hayes, J. M., Small, G. J., & Tiede, D. M. (1989) *J. Phys. Chem. 93*, 5953–5957.

Johnson, S. G., Tang, D., Jankowiak, R., Hayes, J. M., Small, G. J., & Tiede, D. M. (1990) *J. Phys. Chem. 94*, 5849–5855.

Jones, M. R., Visschers, R. W., van Grondelle, R., & Hunter, C. N. (1992) *Biochemistry 31*, 4458–4465.

Jortner, J. (1980) *Biochim. Biophys. Acta 594*, 193–230.

Karplus, M., & McCammon, J. A. (1983) *Annu. Rev. Biochem. 53*, 263–300.

Lauterwasser, C., Finkele, U., Scheer, H., & Zinth, W. (1991) *Chem. Phys. Lett. 183*, 471–477.

Lockhart, D. J., & Boxer, S. G. (1988) *Proc. Natl. Acad. Sci. U.S.A. 85*, 107–111.

Lösche, M., Feher, G., & Okamura, M. Y. (1987) *Proc. Natl. Acad. Sci. U.S.A. 84*, 7537–7541.

Lutz, M., & Mäntele, W. (1991) in *Chlorophylls* (Scheer, H., Ed.) pp 855–902, CRC Press, Boca Raton, FL.

Lyle, P. A., Kolaczkowski, S. V., & Small, G. R. (1993) *J. Phys. Chem. 97*, 6924–6933.

Marcus, R. A., & Sutin, N. (1985) *Biochim. Biophys. Acta 811*, 265–322.

Martin, J.-L., & Vos, M. H. (1992) *Annu. Rev. Biophys. Biomol. Struct. 21*, 199–222.

Martin, J.-L., Breton, J., Hoff, A. J., Migus, A., & Antonetti, A. (1986) *Proc. Natl. Acad. Sci. U.S.A. 83*, 957–961.
Middendorf, T. R., Mazzola, L. T., Gaul, D. F., Schenck, C. C., & Boxer, S. G. (1991) *J. Phys. Chem. 95*, 10142–10151.
Moser, C. C., Keske, J. M., Warncke, K., Farid, R. S., & Dutton, P. L. (1992) *Nature 355*, 796–802.
Palaniappan, V., Aldema, M. A., Frank, H. A., & Bocian, D. F. (1992) *Biochemistry 31*, 11050–11058.
Parson, W. W., Nadebryk, E., & Breton, J. (1992) in *The Photosynthetic Bacterial Reaction Center II* (Breton, J., & Verméglio, A., Eds.) pp 79–88, Plenum, New York.
Schulten, K., & Tesch, M. (1991) *Chem. Phys. 158*, 421–446.
Shreve, A. P., Cherepy, N. J., Franzen, S., Boxer, S. G., & Mathies, R. A. (1991) *Proc. Natl. Acad. Sci. U.S.A. 88*, 11207–11211.
Skourtis, S. S., da Silva, A. J. R., Bialek, W., & Onuchic, J. N. (1992) *J. Phys. Chem. 96*, 8034–8041.
Smith, J. C. (1991) *Q. Rev. Biophys. 24*, 227–291.
Vos, M. H., Lambry, J.-C., Robles, S. J., Youvan, D. G., Breton, J., & Martin, J.-L. (1991) *Proc. Natl. Acad. Sci. U.S.A. 88*, 8885–8889.
Vos, M. H., Lambry, J.-C., Robles, S. J., Youvan, D. G., Breton, J., & Martin, J.-L. (1992) *Proc. Natl. Acad. Sci. U.S.A. 89*, 613–617.
Vos, M. H., Rappaport, F., Lambry, J.-C., Breton, J., & Martin, J.-L. (1993) *Nature 363*, 320–325.
Warshel, A. (1980) *Proc. Natl. Acad. Sci. U.S.A. 77*, 3105–3109.
Warshel, A., & Parson, W. W. (1991) *Annu. Rev. Phys. Chem. 42*, 279–309.
Warshel, A., Chu, Z-T., & Parson, W. W. (1989) *Science 246*, 112–116.
Woodbury, N. W., Becker, M., Middendorf, D., & Parson, W. W. (1985) *Biochemistry 24*, 7516–7521.